Ab initio free energy calculations of the solubility of silica in metallic hydrogen and application to giant planet cores

F. González-Cataldo
[1] *Grupo de NanoMateriales, Departamento de Física, Facultad de Ciencias, Universidad de Chile, Casilla 653, Santiago, Chile*
fgonzalez@lpmd.cl
and

Hugh F. Wilson
Department of Earth and Planetary Science, University of California Berkeley, Berkeley, California 94720, USA
Virtual Nanoscience Laboratory, CSIRO Materials Science and Engineering, Parkville, Victoria 3052, Australia
and

B. Militzer
Department of Earth and Planetary Science, University of California Berkeley, Berkeley, California 94720, USA
Department Astronomy, University of California Berkeley, Berkeley, California 94720, USA

ABSTRACT

By combining density functional molecular dynamics simulations with a thermodynamic integration technique, we determine the free energy of metallic hydrogen and silica, SiO_2, at megabar pressure and thousands of degrees Kelvin. Our *ab initio* solubility calculations show that silica dissolves into fluid hydrogen above 5000 K for pressures from 10 and 40 megabars, which has implication for the evolution of rocky cores in giant gas planets like Jupiter, Saturn and a substantial fraction of known extrasolar planets. Our findings underline the necessity for considering the erosion and redistribution of core materials in giant planet evolution models but also demonstrate that hot, metallic hydrogen is good solvent at megabar pressures, which has implications for high pressure experiments.

Subject headings: planets and satellites: dynamical evolution and stability – planets and satellites: individual (Jupiter, Saturn) – planets and satellites: interiors

1. Introduction

Hydrogen is the simplest and most abundant atom in the universe but its properties at high pressure remain poorly characterized (McMahon et al. 2012). In the interior of giant planets, hydrogen is predicted to occur in metallic form. While such a state has been generated at high temperature with dynamic shock-wave experiments (Weir et al. 1996), obtaining metallic hydrogen in static high pressure experiments at room temperature has been an elusive goal. While the earliest theoretical estimates by Wigner & Huntington (1935) placed an insulator-to-metal transition at only 25 GPa, recent advances in diamond anvil cell experiments (Eremets & Troyan 2011; Howie et al. 2012;

Zha et al. 2012) did not reveal conclusive evidence of metallization for pressures up to approximately 400 GPa. The properties of metallic hydrogen have consequently primarily been studied theoretically (Johnson & Ashcroft 2000) and with *ab initio* computer simulations (Militzer & Graham 2006; Vorberger et al. 2007; Hamel et al. 2011; McMahon et al. 2012; Morales et al. 2013a; Soubiran et al. 2013; Goncharov et al. 2013; Morales et al. 2013b; Becker et al. 2013) that we use also for this article that is focused on the interaction of metallic hydrogen and silica, SiO_2. Silica is not only important for geophysics but also a prototype material for studying condensed matter physics at extreme conditions. Hicks et al. (2006) used shock wave experiments to study the thermodynamic properties of liquid silica at megabar pressures.

In this article we focus on the question whether silica dissolves into metallic hydrogen at megabar pressures because this would have implications for the stability of the cores of solar and extrasolar gas giant planets. Many of the confirmed eight hundred extrasolar planets are gas giants that are primarily composed of dense fluid hydrogen and helium. Furthermore the Kepler mission has detected 2740 planet candidates and has measured their radii and orbital period within 22 months of observations (Batalha et al. 2013). In a few cases with multiple planets in close orbits, masses have been inferred from transit-timing variations (Charbonneau et al. 2009). The Juno mission is scheduled to arrive at Jupiter in 2016 and will measure the gravitational field of our largest local gas giant with an unprecedented accuracy, revealing clues about its inner mass distribution. Existing core-accretion models for gas giants formation (Mizuno et al. 1978) hold that these planets form from the rapid accretion of gas around a rock-ice protocore. Therefore, according to our understanding, the evolution of giant planets starts with a differentiated rocky core surrounded by an envelope of hot, dense hydrogen-helium gas. The temperature in the envelope rises gravitational energy from accretion is converted to heat. An adiabatic temperature is rapidly established. The evolution of a giant planet is controlled by the energy loss due to thermal radiation (Fortney & Nettelmann 2009). Conventional giant planet models assume a stable core and a sharp core-mantle boundary instead of taking into account the possibility that the metallic hydrogen layer may act as solvent for the initial protocore. Answering the question whether giant planet cores remain stable on a billion year time scale may also provide an alternative explanation for the observed heavy element enrichment in giant planet atmospheres, which is currently attributed to late-arriving planetesimals (Niemann et al. 1996; Mahaffy et al. 1998). If a core dissolved it would lead to double diffusive convection (Guillot et al. 2004; Stevenson 1982; Leconte & Chabrier 2012, 2013), because gravity opposes the redistribution of heavy core materials. This would introduce compositional stratification and significantly reduce the rate at which heat can be transported out of the interior, with substantial implications for the thermal evolution and radius contraction of giant planets (Chabrier & Baraffe 2007).

The initial cores of giant planets can be assumed to consist of a combination of rocky and icy materials. The rocky components are likely to be dominated by iron and magnesium silicate minerals. It was shown by Umemoto et al. (2006) that post-perovskite $MgSiO_3$ separates into MgO and SiO_2 beyond $\sim$ 10 megabars and $\sim$ 10000 K, conditions that are expected to be exceeded at the core-mantle boundaries of typical gas giant planets. Recent *ab initio* calculations predicted a substantial solubility of MgO, water ice, and iron in fluid, metallic hydrogen for the core-mantle boundary of Jupiter and Saturn (Wilson & Militzer 2012b,a; Wahl et al. 2013). Therefore this study is focused on the solubility of remaining core material, SiO_2, in order to obtain a more complete picture of the behavior of metallic hydrogen as a solvent of planetary materials.

At the core boundary of giant planets, the temperature and pressure conditions are estimated to be on the order of 10 to 40 Mbar and 10000 to 20000 K. Because such extreme conditions cannot be yet probed with laboratory experiments, we use *ab initio* computer simulations that can be used directly to characterized material at such P-T conditions (Militzer & Wilson 2010; Wilson & Militzer 2010; Militzer 2013; Zhang et al. 2013).

2. Computational Methods

Using density functional molecular dynamics (DFT-MD), we calculated the Gibbs free energy of

solvation, $\Delta G_{\rm sol}$, of SiO_2, given by the difference between the Gibbs free energy of the dissolved system and that of the separate compounds (SiO_2 and hydrogen) at fixed pressure-temperature conditions. We begin by computing the free energy of solvation of SiO_2 for a mixing ratio of one solute atom per 128 hydrogen atoms (i.e. one SiO_2 formula unit to 384 H) and later generalize our results to other concentrations.

$$\Delta G_{\rm sol}(\mathrm{SiO_2}:384\mathrm{H}) = G(\mathrm{H_{384}SiO_2}) - \left[G(\mathrm{H_{384}}) + G(\mathrm{SiO_2})\right]. \quad (1)$$

Given the large quantity of hydrogen gas in giant planets, we are primarily concerned with the low-concentration limit. Thus we can assume that solute atoms do not interact with each other and we introduce the following approximation,

$$G(\mathrm{H_{384}SiO_2}) \approx G(\mathrm{H_{128}Si}) + 2G(\mathrm{H_{128}O}) - k_B T \log(27/2). \quad (2)$$

The last term arises from the free energy of mixing because we do not have the same number of hydrogen atoms in each term.

Since the entropy term in the Gibbs free energies, $G = E + PV - TS$, is not directly accessible in standard molecular dynamics simulations, we used a thermodynamic integration (TDI) technique (Morales et al. 2009; Wilson & Militzer 2012a,b, 2010; Militzer 2013; Sugino & Car 1995) to compute the free energy difference between the system of interest and a simpler non-interacting system whose free energy may be computed explicitly. The difference in Helmholtz free energy between systems governed by two different potentials is given by

$$\Delta F = \int_0^1 \langle U_2 - U_1 \rangle_\lambda \, d\lambda \,, \quad (3)$$

where the angle brackets denotes an average taken over trajectories generated in the system governed by the hybrid potential energy function U_λ. This method provides a general scheme to calculate the Helmholtz free energy difference between two systems governed by potentials $U_1(\mathbf{r_i})$ and $U_2(\mathbf{r_i})$, connected by the hybrid potential $U_\lambda = (1-\lambda)U_1 + \lambda U_2$. Since we have split the Gibbs free energy of solvation in energies of four different systems (pure silica, pure fluid hydrogen, fluid hydrogen with one O atom, and fluid hydrogen with one Si atom), we need to perform four separate sets of simulations at each pressure and temperature. Five equally spaced λ values between 0 and 1 are taken for each of them to get a smooth curve of $(U_2 - U_1)$ vs. λ that can be interpolated via quadratic interpolation to determine the integral. Once we have obtained $\Delta F = F_2 - F_1$, we add the known free energy F_1 to determine the energy of the system, F_2, governed by the potential U_2. The Gibbs free energy is obtained by the addition of the PV term.

The thermodynamic integration is performed in two steps: first, from a system governed by DFT forces to a system interacting via a classical pair potential and then from the classical system to a reference system with a free energy that is known analytically. For fluids, we chose an ideal gas while for solid systems, we selected a system of independent harmonic oscillators as reference system. For the fluid systems, we constructed the classical two-body potentials by fitted to the forces of a DFT-MD trajectory using the force-matching methodology (Izvekov et al. 2004; Tangney & Scandolo 2002). In the case of solid SiO_2 system, we first determined the harmonic spring constants from mean squared displacement from an atom's lattice site and then fitted the residual forces with pair potentials.

The DFT calculations throughout this work were performed using the VASP code (Kresse & Furthmüller 1996). We used pseudopotentials of the projector-augmented wave type (Blochl 1994), the exchange-correlation functional of Perdew, Burke and Ernzerhof (Perdew et al. 1996), a cutoff energy of 900 eV for the plane wave expansion of the wavefunctions, and a $2 \times 2 \times 2$ k-point grid to sample the Brillouin zone, except for the SiO_2 simulations where we used only the Γ point. An MD time step of 0.2 fs was used and the simulation time ranged between 0.5 and 2.0 ps. The $\Delta G_{\rm sol}$ values were confirmed to be well-converged with respect to these parameters for the purpose of this dissolution calculation.

For pure solid SiO_2, we used the Fe_2P-type structure with the space group P-62m that was recently predicted by Tsuchiya & Tsuchiya (2011) to be the ground-state structure at pressures above 7 Mbar. We analyzed stability of each material phase at pressures ranging from 10 to 40 Mbar and temperatures ranging from 3000 to 20000 K and confirmed that the structure remained solid

for all cases under consideration, except for the 20000 K and 20 Mbar where we found liquid SiO_2 to be the stable phase.

Gibbs energies were computed for following system sizes: H_{128}, $H_{128}Si$, $H_{128}O$, solid SiO_2 in a 72-atom supercell, and liquid SiO_2 in a cubic cell with 96 atoms. The resulting Gibbs free energies are shown in Table 1 and plotted as a function of temperature in Fig. 1. The error bars on the G values are dominated by two terms, the more significant one being the uncertainty in the volume at the desired pressure due to finite simulation time, and the other being the uncertainty in the $\langle U_{\rm DFT} - U_{\rm classical} \rangle$ terms in the thermodynamic integration.

3. Results and Discussion

The results in Table 1 are used in conjunction with the equations (1) and (2) to obtain the Gibbs free energies of solvation in Table 2. A negative Gibbs free energy implies that the dissolved state has a lower Gibbs free energy than the separate phases, demonstrating that solvation is preferred at a concentration of 1:384. A positive free energy indicates that the fluid system is supersaturated and that deposition of fluid SiO_2, or formation of solid grains, will be thermodynamically favored. Our results in Fig. 2 are not too different from those found for MgO (Wilson & Militzer 2012a), showing that SiO_2 is also soluble at temperatures that are a bit lower for a given pressure, certainly well below those at Jupiter's core-mantle boundary. This solubility occurs at higher temperatures than water ice (Wilson & Militzer 2012b), where the solubility was already strongly favored at much lower temperatures of 2000-3000 K in the same pressure range.

Gibbs free energy of solvation can be generalized to other concentrations without performing additional DFT-MD simulations if the average separation between solute atoms is large enough so that their interaction can be neglected. Under this assumption, the free energy of mixing yields the difference of $\Delta G_{\rm sol}$ between a solution of one SiO_2 formula unit in m versus n hydrogen atoms (Wilson & Militzer 2012b),

$$\frac{\Delta G_{\rm sol}[m] - \Delta G_{\rm sol}[n]}{k_B T} = m \ln\left(\frac{m V_{\rm H} + V_{\rm Si} + 2V_{\rm O}}{m V_{\rm H}}\right) - n \ln\left(\frac{n V_{\rm H} + V_{\rm Si} + 2V_{\rm O}}{n V_{\rm H}}\right) + 3 \ln\left(\frac{m V_{\rm H} + V_{\rm Si} + 2V_{\rm O}}{n V_{\rm H} + V_{\rm Si} + 2V_{\rm O}}\right),$$

where $V_{\rm H}$, $V_{\rm O}$ and $V_{\rm Si}$ are the effective volumes of the H, O, and Si atoms that we obtained by comparing the volumes of the different fluid simulations at same pressure and temperature. Using a linear interpolation for the data in Table 2, we can determine the saturation concentration for SiO_2 in fluid hydrogen as a function of temperature and pressure throughout the 10–40 Mbar and 3000–20000 K range. A contour plot of constant saturation solubility is shown in Fig. 2. Solute concentrations higher than 1:100 are not shown because they may lead to interactions between solute atoms. Despite of an error bars of approximately 1000 K that should be considered to be uncertainties of the contours, these results show that SiO_2 is highly soluble at both Jupiter's and Saturn's core-mantle boundary conditions. This is in contrast to MgO, which may be not be as highly soluble at Saturnian core conditions. Therefore, there exists the possibility that SiO_2 may dissolve

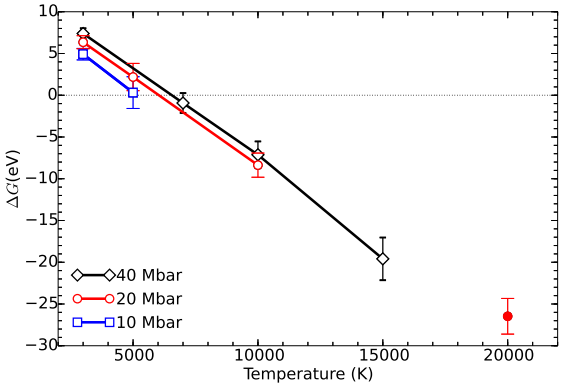

Fig. 1.— (Color online) Computed solvation curve ΔG for different pressures, where negative Gibbs free energy represents a preference for the dissolved state. Open squares, circles and diamonds represent states where SiO_2 is solid, while the filled red circle corresponds to a state where SiO_2 was found to be liquid.

from Saturn's core but leave solid MgO behind.

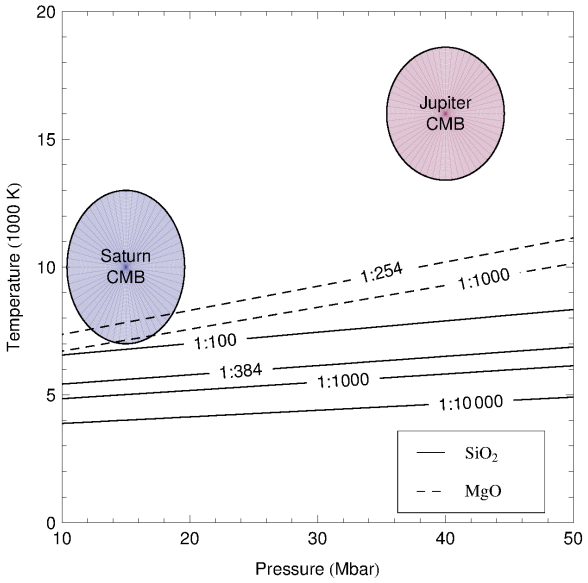

Fig. 2.— Saturation solubility of SiO_2 in metallic hydrogen (this work; solid lines) and MgO (from Wilson & Militzer (2012a); dashed lines) as a function of temperature and pressure. The temperature-pressure conditions of the Jovian and Saturnian core-mantle boundaries are shown for comparison.

The Gibbs free energy of solubility ΔG may be split into three components: an internal energy component ΔU, a volume contribution $P\Delta V$ and an entropic term $-T\Delta S$, which lead to $\Delta G = \Delta U - T\Delta S + P\Delta V$. The $P\Delta V$ and ΔU values can be directly extracted from standard DFT-MD simulations. The remaining term is $-T\Delta S$ from calculated ΔF. All terms are shown in Fig. 3 as a function of temperature at 20 Mbar. The $P\Delta V$ term was comparatively close to zero but shows a slight preference of approximately 0.5–3.5 eV for materials to remain separate, suggesting the dissolution reaction is not a pressure-driven process. The ΔU term also shows an energy barrier against dissolution that is slightly larger than the $P\Delta V$ term. For all temperatures under consideration, the entropic term $-T\Delta S$ is negative, confirming that more disorder is present in the dissolved state. The $-T\Delta S$ term exhibits a steep negative slope as a function temperature that introduces a sign change into the Gibbs energy balance at T=6000 K for 20 Mbar where SiO_2 is solid. Above this temperature, dissolution is favored, which can be considered to be an entropy-driven process similar to H_2O and MgO (Wilson & Militzer 2012b,a). For iron, $-T\Delta S$ term also favors dissolution but there is no energy barrier to overcome because at megabar pressures, hydrogen and iron are both metals that mix at low temperature (Wahl et al. 2013).

Figure 3 shows that the Gibbs free energy of solubility depends linearly on temperature. This trend continues into the liquid phases as our data point as 20 000 K confirms. For the temperature interval from 10 000 and 20 000 K where one expects SiO_2 to melt at 20 Mbar (González-Cataldo et al. 2014), this trend implies that the Gibbs free energy difference between the solid and liquid phases is small compared to Gibbs free energy change induced by dissolution. If SiO_2 melts in the vicinity of the dissolution transition, one would expect this transition to introduce only a modest change in slope into saturation solubility curves in Fig. 2 because the Gibbs free energy changes continuously across the melting transition.

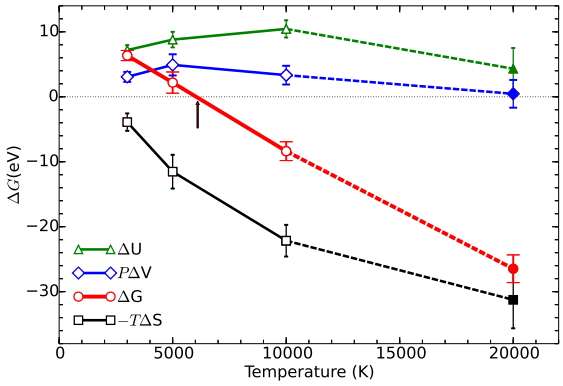

Fig. 3.— (Color online) Splitting of ΔG at 20 Mbar into its three constituent components: the internal energy term ΔU that represents differences in chemical binding, the $P\Delta V$ term that arises from volume differences, and the remaining $-T\Delta S$ term which represents entropic effects. The arrow marks the temperature above which dissolutions favored at concentration of one SiO_2 in 384 hydrogen atoms.

4. Conclusions

The presented *ab initio* free energy calculations demonstrate that metallic hydrogen is a good solvent for silica at megabar pressures for temperatures above 5000 K. This result is consistent with recent *ab initio* solubility calculations that predicted H_2O to dissolve into metallic hydrogen at 2000 to 3000 K (Wilson & Militzer 2012b) and MgO at 6000 to 8000 K (Wilson & Militzer 2012a). This suggests other insulating materials may dissolve at a comparable temperature range. Iron was found to dissolve at low temperature because it is a metal (Wahl et al. 2013). These findings suggest that hydrogen will spontaneously react with any material that is used as confinement during dynamic shock wave experiments that reach megabar pressure and high temperatures. Our findings indirectly places a limit on the time scale of such experiments before a significant contamination of sample sets in.

Our results also have implications for the evolution of giant planets. We predict that the SiO_2 component has been eroded from the cores of Jupiter and Saturn while MgO in Saturn's core may remain stable. Therefore a partial solvation of the Saturnian core could have taken place, taking away more volatile materials like SiO_2 and water ice, leaving behind less soluble materials like MgO. Because of the differences between the solubility curves of MgO and SiO_2 in Fig. 2, partial core erosion may also occur in extrasolar gas giant planets that are smaller than Saturn but still large enough to contain metallic hydrogen. In genernal, larger, hotter interiors are expected to promote core erosion and a greater degree of redistribution of heavy material (Guillot et al. 2004). Provided the necessary energy for convection, the material may be redistributed throughout the entire planet, leading to an enrichment in heavy elements in giant planets atmospheres that have previously been attributed to late-arriving planetesimals.

Alternatively, the rate of redistribution may be hampered by compositional stratification that is the result of double diffusion convection (Guillot et al. 2004; Stevenson 1982; Leconte & Chabrier 2012). The stratification would also limit the heat transport from the core, delay a planet's cooling, and possibly explain the inflated radii that have been observed for a large of number giant exoplanets (Chabrier & Baraffe 2007).

We have assumed that there is sufficient hydrogen available for the approximation of noninteracting solute atoms to remain valid. Also other stoichiometries of SiO_2 have not been considered, assuming Si and O to dissolve in a one-to-two ratio according to the charge balance.

Our results confirm that the core erosion must be taken into account when future models of giant planet interiors are constructed. The redistribution of heavy element has important implications in the heat transport and mass distribution, and core erosion plays a fundamental role in this aspect, since it may be the source of the presence of these elements in the outer layers. Further models for the upconvection of core material are also necessary to understand the present structure of Jupiter and other planets, whose effects may be reflected on the gravitational moments to be measured by the Juno mission.

F.G.-C. acknowledges the PhD fellowship from CONICYT and short-term fellowship from Universidad de Chile, Chile. H.F.W. and B.M. received support from NASA and NSF.

REFERENCES

Batalha, N. M., Rowe, J. F., Bryson, S. T., et al. 2013, The Astrophysical Journal Supplement Series, 204, 24, updated at http://www.nasa.gov/mission_pages/kepler

Becker, A., Nettelmann, N., Holst, B., & Redmer, R. 2013, Phys. Rev. B, 88, 045122

Blochl, P. E. 1994, Phys. Rev. B, 50, 17953

Chabrier, G., & Baraffe, I. 2007, Astrophys. J., 661, L81

Charbonneau, D., Berta, Z. K., Irwin, J., et al. 2009, Nature, 462, 891

Eremets, M. I., & Troyan, I. A. 2011, Nat. Mater., 10, 927

Fortney, J. J., & Nettelmann, N. 2009, Space Science Reviews, 152, 423

Goncharov, A. F., Tse, J. S., Wang, H., et al. 2013, Phys. Rev. B, 87, 024101

González-Cataldo, F., Davis, S., & Gutiérrez, G. 2014, Proceedings of the National Academy of Sciences of the United States of America, submitted

Guillot, T., Stevenson, D. J., Hubbard, W. B., & Saumon, D. 2004, The interior of Jupiter, ed. F. Bagenal, T. E. Dowling, & W. B. McKinnon (Cambridge University Press), 35–57

Hamel, S., Morales, M. A., & Schwegler, E. 2011, Phys. Rev. B, 84, 165110

Hicks, D. G., Boehly, T. R., Eggert, J. H., et al. 2006, Phys. Rev. Lett., 97, 025502

Howie, R. T., Guillaume, C. L., Scheler, T., Goncharov, A. F., & Gregoryanz, E. 2012, Phys. Rev. Lett., 108, 125501

Izvekov, S., Parrinello, M., Burnham, C. J., & Voth, G. A. 2004, J. Chem. Phys., 120, 10896

Johnson, K. A., & Ashcroft, N. W. 2000, Nature, 403, 632

Kresse, G., & Furthmüller, J. 1996, Phys. Rev. B, 54, 11169

Leconte, J., & Chabrier, G. 2012, Astronomy & Astrophysics, 540, A20

—. 2013, Nature Geoscience, 6, 347

Mahaffy, P. R., Niemann, H. B., Alpert, A., et al. 1998, Bull. Am. Astron. Soc., 30, 1066

McMahon, J. M., Morales, M. A., Pierleoni, C., & Ceperley, D. M. 2012, Rev. Mod. Phys., 84, 1607

Militzer, B. 2013, Phys. Rev. B, 87, 014202

Militzer, B., & Graham, R. L. 2006, Journal of Physics and Chemistry of Solids, 67, 2136

Militzer, B., & Wilson, H. F. 2010, Phys. Rev. Lett., 105, 195701

Mizuno, H., Nakazawa, K., & Hayashi, C. 1978, Prog. Theor. Phys., 60, 699

Morales, M. A., Hamel, S., Caspersen, K., & Schwegler, E. 2013a, Phys. Rev. B, 87, 174105

Morales, M. A., McMahon, J. M., Pierleoni, C., & Ceperley, D. M. 2013b, Phys. Rev. B, 87, 184107

Morales, M. A., Schwegler, E., Ceperley, D., et al. 2009, PNAS, 106, 1324

Niemann, H. B., Atreya, S. K., Carignan, G. R., et al. 1996, Science, 272, 846

Perdew, J. P., Burke, K., & Ernzerhof, M. 1996, Phys. Rev. Lett., 77, 3865

Soubiran, F., Mazevet, S., Winisdoerffer, C., & Chabrier, G. 2013, Phys. Rev. B, 87, 165114

Stevenson, D. J. 1982, Planet. Space. Sci, 30, 755

Sugino, O., & Car, R. 1995, Physical Review Letters, 74, 1823

Tangney, P., & Scandolo, S. 2002, The Journal of Chemical Physics, 117, 8898

Tsuchiya, T., & Tsuchiya, J. 2011, Proceedings of the National Academy of Sciences of the United States of America, 108, 1252

Umemoto, K., Wentzcovitch, R. M., & Allen, P. B. 2006, Science, 311, 983

Vorberger, J., Tamblyn, I., Militzer, B., & Bonev, S. 2007, Phys. Rev. B, 75, 024206

Wahl, S. M., Wilson, H. F., & Militzer, B. 2013, Astrophys. J., 773, 95

Weir, S., Mitchell, A., & Nellis, W. 1996, Phys. Rev. Lett., 76, 1860

Wigner, E., & Huntington, H. B. 1935, J. Chem. Phys., 3, 764

Wilson, H., & Militzer, B. 2012a, Physical Review Letters, 108, 111101

Wilson, H. F., & Militzer, B. 2010, Phys. Rev. Lett., 104, 121101

—. 2012b, Astrophys. J., 745, 54

Zha, C. S., Liu, Z., & Hemley, R. J. 2012, Phys. Rev. Lett., 108, 146402

Zhang, S., Wilson, H. F., Driver, K. P., & Militzer, B. 2013, Physical Review B, 87, 024112

This 2-column preprint was prepared with the AAS LaTeX macros v5.2.

Table 1

Gibbs free energies of pure hydrogen, hydrogen with oxygen, hydrogen with silicon, and SiO_2 (solid in all cases, except for 20 Mbar and 20000 K).

P, T (Mbar, 1000K)	$G(H_{128})$ (eV)	$G(H_{128}O)$ (eV)	$G(H_{128}Si)$ (eV)	G (SiO_2) (eV)
10, 3	671.4(2)	688.6(2)	705.4(3)	63.3(1)
10, 5	559.0(5)	573.5(4)	590.5(5)	60.2(1)
20, 3	1270.7(2)	1304.7(2)	1330.1(3)	121.0(1)
20, 5	1170.8(4)	1202.4(5)	1228.2(3)	118.4(1)
20, 10	843.2(4)	868.3(4)	893.8(2)	109.1(4)
20, 20	17.3(5)	26.9(6)	53.6(7)	81.8(1)
40, 3	2131.4(2)	2191.8(2)	2229.4(1)	211.3(1)
40, 7	1936.2(3)	1991.4(3)	2030.7(3)	206.0(2)
40, 10	1747.4(1)	1799.0(6)	1837.6(9)	200.6(3)
40, 15	1384.3(8)	1427.9(4)	1467.6(8)	190.1(4)

Table 2

Gibbs free energies of solubility for SiO_2 into hydrogen at a concentration of one part in 384 hydrogen atoms.

P (Mbar)	T (K)	ΔG_{sol} (eV)
10	3000	4.92 ± 0.69
10	5000	0.32 ± 1.90
20	3000	6.35 ± 0.78
20	5000	2.18 ± 1.63
20	10000	-8.37 ± 1.45
20	20000	-26.47 ± 2.14
40	3000	7.40 ± 0.63
40	7000	-0.93 ± 1.19
40	10000	-7.13 ± 1.60
40	15000	-19.59 ± 2.55